Available online at www.sciencedirect.com
SCIENCE DIRECT®
Journal of Molecular Graphics and Modelling 22 (2003) 55–70
Journal of Molecular Graphics and Modelling
www.elsevier.com/locate/JMGM

Modeling and molecular dynamics of glutamine transaminase K/cysteine conjugate β-lyase

Jennifer Venhorst, Antonius M. ter Laak, Moira Meijer, Ineke van de Wetering, Jan N.M. Commandeur, Martijn Rooseboom, Nico P.E. Vermeulen*

Department of Pharmacochemistry, Division of Molecular Toxicology, Leiden/Amsterdam Center for Drug Research (LACDR), Vrije Universiteit, De Boelelaan 1083, 1081 HV Amsterdam, The Netherlands

Received 20 September 2002; received in revised form 28 February 2003; accepted 5 March 2003

Abstract

The homodimeric, pyridoxal 5′-phosphate (PLP)-dependent enzyme glutamine transaminase K/cysteine conjugate β-lyase (GTK/β-lyase) has been implicated in the bioactivation of chemopreventive compounds. This paper describes the first homology model of rat renal GTK/β-lyase and its active site residues, deduced from molecular dynamics (MD) simulations of the binding mode of 13 structurally diverse cysteine *S*-conjugates and amino acids after Amber-parametrization of PLP. Comparison with *Thermus thermophilus* aspartate aminotransferase (tAAT) and *Trypanosoma cruzi* tyrosine aminotransferase (tTAT), used as templates for modeling GTK/β-lyase, showed that the PLP-binding site of GTK/β-lyase is highly conserved. Binding of the ligand α-carboxylate-group occurred via the conserved residues Arg^{432} and Asn^{219}, and Asn^{50} and Gly^{70}. Two pockets accommodated the various ligand side chains. A small pocket, located directly above PLP, was of a highly hydrophobic and aromatic character. A larger pocket, formed partly by the substrate access channel, was more hydrophilic and notably involved the salt bridge partners Glu^{54} and Arg^{99*} (∗ denotes the other subunit). Ligand-binding residues included Leu^{51}, Phe^{71}, Tyr^{135}, Phe^{373} and Phe^{312*}, and π-stacking interactions were often observed. Tyr^{135} and Asn^{50} were prominent in hydrogen bonding with the sulfur-atom of cysteine *S*-conjugates.

The observed binding mode of the ligands corresponded well with their experimentally determined inhibitory potency toward GTK/β-lyase. The current homology model thus provides a starting point for further validation of the role of active site residues in ligand-binding by means of mutagenesis studies. Ultimately, insight in the binding of ligands to GTK/β-lyase may result in the rational design of new ligands and selective inhibitors.

Keywords: Glutamine transaminase K/cysteine conjugate β-lyase; PLP-dependent enzymes; Comparative modeling; Molecular dynamics; Active site topology; PLP-parametrization

1. Introduction

Glutamine transaminase K/cysteine conjugate β-lyase (GTK/β-lyase), first discovered by Cooper and Meister [1], is a pyridoxal-5′-phosphate (PLP)-dependent enzyme of approximately 48 kDa, located among others in the human and rat kidney cytosol [2,3]. GTK/β-lyase belongs to the α-family of the superfamily of PLP-dependent enzymes, and has also been classified to the γ-group of the aminotransferase I (AT I) subfamily [4,5]. Proteins belonging to the α-family of PLP-dependent enzymes are dimers composed of two identical subunits, each containing one equivalent of PLP. In the resting state, PLP is covalently bound to the ε-nitrogen atom of an active site lysine residue, forming an internal aldimine (Fig. 1). Like all aminotransferases, GTK/β-lyase catalyzes a reversible interconversion of amino acids and α-keto-acids (pathway B, Fig. 1). The cofactor PLP hereby functions as an amino-group acceptor [6,7]. GTK/β-lyase may thus play an important role in preserving the physiological amino acid balance, where the dietary non-essential glutamine is used to maintain the tissue levels of other amino acids and to prevent the loss of essential α-keto-acids [1]. Another reaction pathway catalyzed by GTK/β-lyase is the β-elimination of *S*-conjugates and *Se*-conjugates of L-(seleno)cysteine, resulting in the cleavage of the C–S or C–Se bond (pathway A, Fig. 1). Due to this reaction route, GTK/β-lyase is also referred to as a cysteine conjugate β-lyase [8,9].

Each subunit of the homodimeric α-family members of PLP-dependent enzymes consists of an N-terminal segment, a small domain, and a large domain [7,10]. The topology

* Corresponding author. Tel.: +31-20444-7590; fax: +31-20444-7610.
E-mail address: vermeule@chem.vu.nl (N.P.E. Vermeulen).

1093-3263/03/$ – see front matter © 2003 Published by Elsevier Science Inc.
doi:10.1016/S1093-3263(03)00136-0

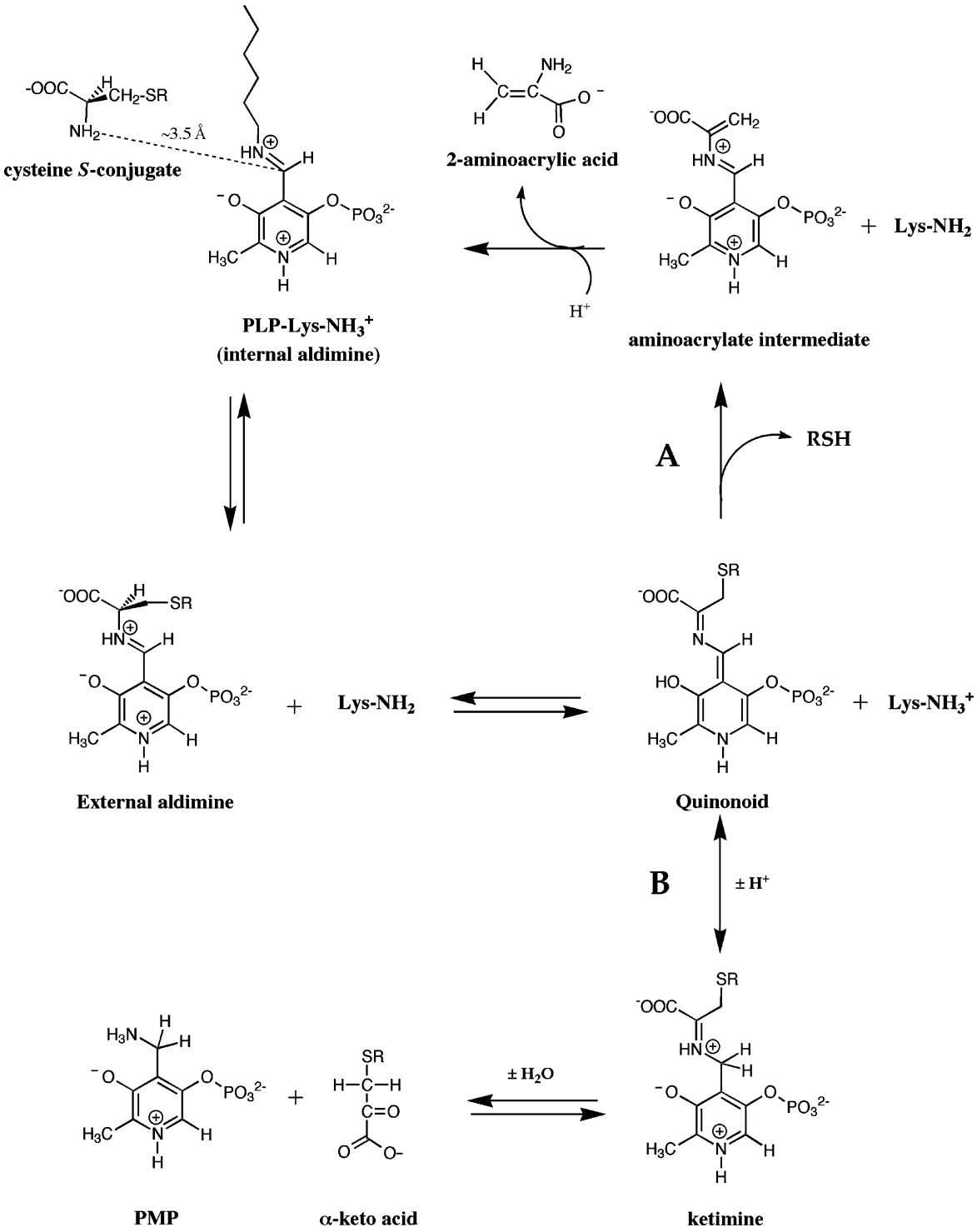

Fig. 1. Catalytic cycle of glutamine transaminase K/cysteine conjugate β-lyase for the β-elimination (A) and transamination pathway (B), shown here for a L-cysteine *S*-conjugate [6,7].

of the large domain is most conserved, and consists of an α/β/α-sandwich. The seven-stranded β-sheet of the large domain is invariant, its strands being parallel with the exception of strand f. However, the number of α-helices surrounding the β-sheet varies between α-family members. The small domain possesses an α/β-structure and differs between α-family members both in the number of β-sheets and α-helices. The topology of the N-terminal segment differs even between groups of an α-family member, and can be as diverse as an extended coil and an α/β-structure [11,12]. The active site and PLP-binding site of α-family proteins are located at the subunit- and domain-interface of the dimer.

GTK/β-lyase is of interest both from a toxicological and pharmacological perspective. Extensive studies on β-eliminating enzymes including GTK/β-lyase were initially performed because of the observed selective nephrotoxicity of halogenated alkenes, which arises from β-elimination of the corresponding cysteine *S*-conjugates to reactive thiols [8]. The formation of *S*-conjugates is mediated by glutathione *S*-transferases and hydrolases, and the resulting *S*-conjugates are actively taken up in the kidney, accounting for the organ selective toxicity [8]. More recently, several *S*- and *Se*-conjugates of, respectively, L-cysteine and L-selenocysteine, e.g. *S*-allyl-L-cysteine and *Se*-methyl-L-selenocysteine, have been demonstrated to exert chemoprotective [13] and chemopreventive actions [14–16]. In a study by Ip et al. [17], the chemopreventive activity of some L-selenocysteine *Se*-conjugates has been attributed to the release of biologically active selenols upon β-lyase-mediated scission of the C–Se bond. Selenocysteine *Se*-conjugates undergo β-elimination by GTK/β-lyase with extremely high catalytic efficiency, up to 200 times higher than that observed for the corresponding cysteine *S*-conjugates [18]. GTK/β-lyase may thus serve as a target to locally bioactivate prodrugs. The kidney-selective release of anti-tumorigenic selenols has already been suggested as a therapeutic application [19].

Given the variety of biological effects mediated by substrates of GTK/β-lyase, knowledge of the active site topology of GTK/β-lyase on a molecular level, and its mode of substrate binding, is highly valuable. To date, the crystal structure of GTK/β-lyase has not been resolved and insight in structure–function relationships of GTK/β-lyase has solely been derived from metabolism studies [18]. In the absence of an experimentally determined 3D-structure, valuable information on active site topologies can be inferred from homology models [20]. Due to the crystallization and 3D-structure elucidation of homologous proteins [21,22], this approach is now also possible for GTK/β-lyase. In the current study, we describe the development of the first protein model of rat GTK/β-lyase, using comparative modeling techniques. The rat renal enzyme was modeled, as we were able to experimentally validate this homology model. Molecular dynamics (MD) studies were performed on ligand–protein complexes in order to identify ligand-interaction residues and to rationalize the observed affinity of ligands for GTK/β-lyase. Insight in the binding site of GTK/β-lyase may ultimately lead to the rational design of selective substrates and inhibitors. The latter are currently not available.

2. Materials and methods

2.1. Chemicals and protein

α-Keto-γ-methiolbutyrate, L-glutamine, and *S*-benzyl-L-cysteine were purchased from Sigma Chemical Co. (St. Louis, MO). *o*-Phenylenediamine and D/L-phenylalanine were obtained from Janssen Chimica (Geel, Belgium). Pyruvate, *S*-carbamyl-L-cysteine, and *S*-methyl-L-cysteine were from Aldrich (Steinheim, Germany). *S*-(4-Methylbenzyl)-L-cysteine and *S*-(4-methoxybenzyl)-L-cysteine were, respectively, obtained from Advanced Chem. Tech. (Louisville, KY) and Bachem Feinchemikalien AG (Bubbendorf, Switzerland). *S*-Phenyl-L-cysteine, *S*-(4-methoxyphenyl)-L-cysteine and *Se*-(4-methylbenzyl)-L-selenocysteine were prepared as described by Andreadou et al. [19]. The substituted *S*-nitrophenyl conjugates *S*-(2,4-dinitrophenyl)-L-cysteine, *S*-(2-nitrophenyl)-L-cysteine and *S*-(4-carboxy-2-nitrophenyl)-L-cysteine were synthesized according to the procedures described by Blaghbrough et al. [24]. GTK/β-lyase was purified 1036-fold from rat kidney cytosol with the procedure by Yamauchi et al. [23].

2.2. Model building and structure refinement

The primary sequence of rat renal GTK/β-lyase (accession number Q08145) was obtained from the Sequence Retrieval System (SRS) accessible from the EMBL internet site (Heidelberg, Germany). A search for homologous sequences with resolved crystal structure was carried out using the EMBL Fasta3 search engine.

A structure alignment of homologues of GTK/β-lyase was made manually using the homology module of InsightII (Biosym, San Diego). The resulting consensus, in combination with the secondary structure prediction for GTK/β-lyase obtained with the PHDsec program [25,26], was used to manually align the sequence of GTK/β-lyase. The quality of the obtained alignment was subsequently scrutinized on the basis of the resulting consensus and structural conservation between templates. Structure elements were designated of “high” or “excellent” quality when good structural overlap existed between the templates. Elements qualified as “excellent” additionally contained at least two conserved residues or a conserved PLP- or ligand-binding residue (Table 1). Structure elements classified as “high” in quality contained at least one conserved residue or was located between highly conserved regions. The designation “fair” was used for structure elements that either had a less clear consensus or were located near parts that were more variable in the template structures. Finally, the “low” quality designation was used for structure elements which both lacked a clear consensus and good overlap between the templates.

Ten different 3D-models of the dimeric apoprotein of GTK/β-lyase were generated with the restraint-based comparative modeling program Modeller 4.0 [27]. Dimeric units of the structurally resolved aminotransferases with PDB-identifiers 1BKG (*Thermus thermophilus* aspartate aminotransferase (tAAT)) and 1BW0 (*Trypanosoma cruzi* tyrosine aminotransferase (tTAT)) were used as templates. Aspartate aminotransferases (AATs) are known to transform from an open to closed conformation upon substrate

Table 1
Proposed functional roles of conserved residues in rat GTK/β-lyase located in the PLP- and ligand-binding site as inferred from homologous proteins [5,10,44]

Location	Residue	Functional role	Conservation level
PLP-binding site	Lys^{281}	Internal aldimine formation	α-Family
	Asp^{247}	Salt bridge with pyridinium N PLP	α-Family
	Asn^{219}	H-bond with phenolic O PLP	AT I subfamily[a]
	Tyr^{250}	H-bond with phenolic O PLP	AT I subfamily[a]
	Lys^{289}	Salt bridge with phosphate PLP	γ-Group[b]
	Tyr^{97*}	H-bond with phosphate PLP	AT I subfamily[a]
Ligand-binding site	Asn^{219}	H-bond with α-carboxylate ligands	AT I subfamily[a]
	Arg^{432}	Salt bridge with α-carboxylate ligands	α-Family

[a] Some exceptions are known and have been described by Jensen and Gu [5].
[b] Conserved as a positively charged arginine or lysine in the AT I subfamily.
* Denotes a residue originating from the other subunit.

binding [11,28]. In the case of tAAT, this movement only involves the N-terminal region of the small domain [21,29]. As we aimed to model the ligand-bound conformation of GTK/β-lyase (the protonated internal aldimine in Fig. 1), we have used the closed conformation of tAAT (PDB-identifier 1BKG) instead of the crystallized open conformation (PDB-identifier 1BJW). The model with the best loop conformations and stereochemical parameters as determined by PROCHECK [30], was used for further modeling.

As both template structures were crystallized with pyridoxamine 5′-phosphate (PMP, Fig. 1) instead of PLP, the coenzyme was extracted from 1BJW and fitted in the PLP-binding site of each monomer as the protonated aldimine. To relax the structure and optimize the cofactor–enzyme interactions an optimization was carried out with Amber 5.0 using the minimization procedure described below, with harmonic restraints ($k = 1$ kcal/(mole Å^2)) applied on the protein backbone and conserved cofactor–enzyme interactions (Table 1).

2.3. Structure generation and charge calculations of ligands

For the purpose of identifying potential ligand-interaction residues of the rat GTK/β-lyase homology model, docking studies were performed with a set of L-cysteine-*S*-conjugates and the endogenous compounds glutamine and phenylalanine (Fig. 2). Selection of the investigated ligands was based on structural diversity and the ability to determine the inhibitory potency of the compounds toward rat GTK/β-lyase. Both L- and D-phenylalanine were included to investigate the reported stereoselectivity of GTK/β-lyase toward L-amino acids [3].

Initial structures of the ligands studied were generated and minimized with the Xleap module of Amber 5.0. Atomic charges of the substrates were essentially derived as described by Cieplak et al. [31]. In short, conformational analyses and subsequent hierarchical clustering were performed with Sybyl 6.7 (Tripos Inc., St. Louis, Missouri) to obtain the four minimum energy geometries covering the broadest range of the conformational space of each ligand. Electrostatic potentials were subsequently calculated for all four conformers at the Connolly surface at 1.4, 1.6, 1.8, and 2 times the Van der Waals radius using GAMESS US and the SV 6–31G* basis set. The multiconformational restraint electrostatic potential (RESP)-fitting procedure [32,33] was utilized to obtain atomic charges. The same procedure was subsequently followed to derive atomic charges for the protonated internal aldimine form of PLP, of which the results are shown in Table 2. Charges for the unprotonated internal aldimine were also derived (Table 2).

2.4. Ligand docking and molecular dynamics

Low energy conformers of each ligand were manually docked in the active site of both GTK/β-lyase subunits in an orientation similar to that described for ligands of tTAT [22] using InsightII (Biosym, San Diego, CA). The α-carboxylate-group of each ligand was placed within hydrogen bonding distance to both Arg^{432} and Asn^{219}. The amino-group of each ligand was simultaneously positioned at a distance of approximately 3.5 Å from the reactive center of PLP: the aldimine carbon atom C4A. The side chain of the different ligands was oriented such as to obtain maximum overlap with each other whenever possible in order to obtain comparable starting structures of the ligand–enzyme complexes. Torsion angles of ligands and protein side chains were varied when necessary, to eliminate steric clashes. The starting structure of each complex was minimized with Amber 5.0 for 20,000 steps, first using the steepest descent method followed by the conjugate gradient minimizer. In all calculations, a dielectric constant of 1 and cutoff of 8 Å were used. During the minimization, the protein backbone was restraint by a harmonic function with a force constant of 1 kcal/(mole Å^2). In addition, distance restraints ($k = 50$ kcal/(mole Å^2)) were applied on conserved hydrogen bonds between PLP and the apoprotein, and between the ligand and the enzyme (Table 1). Molecular dynamics

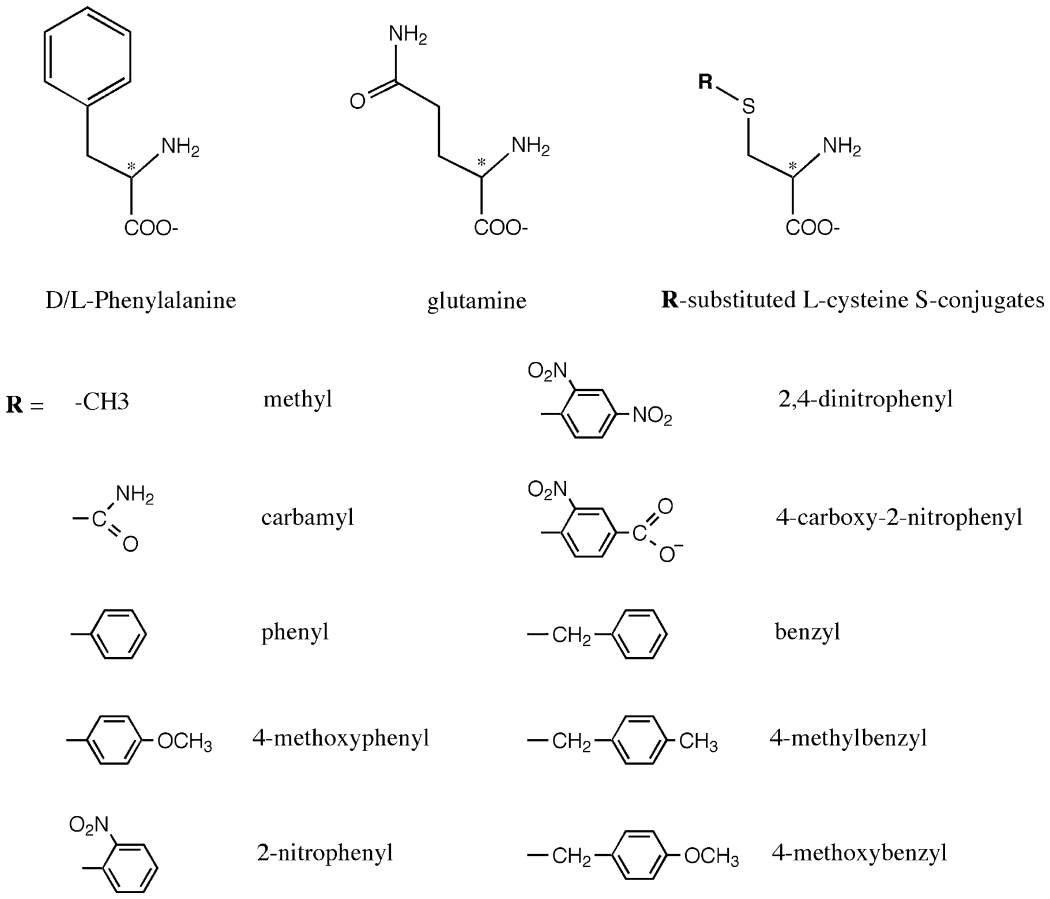

Fig. 2. Structure of the ligands, that were docked in the GTK/β-lyase active site. The ligands were docked with neutral amino-group to mimic the protonated internal aldimine intermediate of rat GTK/β-lyase as shown in Fig. 1.

was subsequently performed on the minimized structures at 300 K for a total of 100 ps to optimize the ligand–enzyme interactions. During the first 20 ps, the distance restraints used in the minimization procedure were also applied during the MD run. In the subsequent 20 ps, the force constant applied on these distance restraints was gradually reduced from 50 to 0 kcal/(mole Å^2)). During the last 60 ps, the substrates and cofactor were completely free to move. Due to the size of the system, no explicit water molecules were included in the simulations. As such, solvent effects were not taken into account. A weak harmonic restraint of 1 kcal/(mole Å^2) was applied on the Cα-trace of the protein during the MD run. A similar approach, i.e. ligand docking studies in the absence of water and with a restraint backbone, has previously been used for tTAT [22]. The final structure resulting from the MD run was minimized without any restraints, using the conditions described above. For each ligand several simulations were carried out, which differed in the starting orientation of the ligand. The representative binding mode of the ligand, described in the results and discussion, was considered to be the one with the highest average interaction energy calculated over the last 50 ps of each MD run.

2.5. Competition studies

Competition studies were performed by measuring the inhibition of pyruvate formation from GTK-mediated β-elimination of *Se*-(4-methylbenzyl)-L-selenocysteine by the cysteine *S*-conjugates and amino acids shown in Fig. 2. Of known selenocysteine-*Se*-conjugates, *Se*-(4-methylbenzyl)-L-selenocysteine is β-eliminated by GTK/β-lyase at the highest rate [18]. Incubations (0.1 ml) containing 0.5 mM *Se*-(4-methylbenzyl)-L-selenocysteine, 0.5 μg/ml purified GTK/β-lyase, and 0.5 mM α-keto-γ-methiolbutyrate (KMB; cofactor) were incubated in the absence or presence of 0.1, 0.3, 1, and 3 mM cysteine *S*-conjugate in 50 mM sodium borate buffer (pH 8.6) at 37 °C. After 0 and 10 min the reaction was terminated by adding 0.2 ml of 0.14% *o*-phenylenediamine in 3 N HCl. Samples were heated for 60 min at 60 °C to derivatize pyruvate with the α-keto-acid reagent *o*-phenylenediamine. After cooling down to room temperature, 300 μl of HPLC-eleunt was added after which the solution was transferred to HPLC-vials. Samples were analyzed by HPLC, using two 100 × 3 mm ChromSpher 5 C18-columns (Varian, Europe) with isocratic elution using

Table 2
Atomic charges derived for the protonated and unprotonated internal aldimine form of the cofactor, where pyridoxal 5′-phosphate is covalently bound to an active site lysine

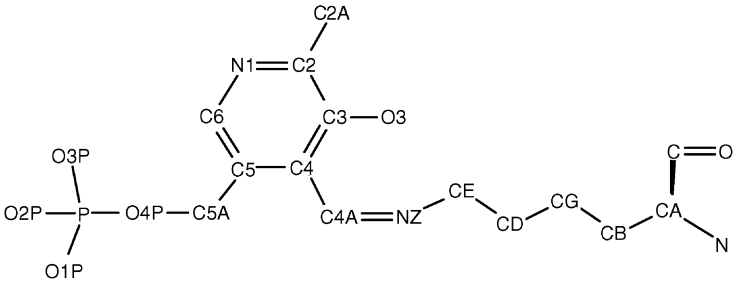

Heavy atom	Atomic charge		Connected H-atom	Atomic charge	
	Protonated	Unprotonated		Protonated	Unprotonated
N1	−0.212000	−0.242353	H1	0.345500	0.321881
C2	0.205800	0.145003			
C3	0.355700	0.380924			
O3	−0.765500	−0.789120			
C4	0.102000	0.086085			
C5	−0.173800	−0.184993			
C6	−0.099200	−0.143832	H6	0.191900	0.158789
C2A	−0.279000	−0.239231	H2A1	0.096900	0.067671
			H2A2	0.096900	0.067671
			H2A3	0.096900	0.067671
C4A	0.102300	0.124096	H4A	0.205400	0.052020
C5A	0.349900	0.514861	H5A1	0.008300	−0.067891
			H5A2	0.008300	−0.067891
O4P	−0.538200	−0.519343			
P	1.243900	1.209318			
O1P	−0.882100	−0.895327			
O2P	−0.882100	−0.895327			
O3P	−0.882100	−0.895327			
NZ	−0.139900	−0.256498	HZ	0.381900	–
CE	0.115600	0.473158	HE2	−0.011400	−0.173431
			HE3	−0.011400	−0.173431
CD	0.109400	0.314178	HD2	−0.005800	−0.106832
			HD3	−0.005800	−0.106832
CG	0.062900	0.021389	HG2	−0.078200	−0.121812
			HG3	−0.078200	−0.121812
CB	0.499500	0.818672	HB2	−0.114700	−0.215839
			HB3	−0.114700	−0.215839
CA	−0.441900	−0.556790	HA	0.110200	0.098816
C	0.734100	0.734100			
O	−0.589400	−0.589400			
N	−0.347900	−0.347900	H	0.274700	0.274700

Charges were derived by the restraint electrostatic potential (RESP)-fitting procedure described by Bayly et al. [32] and Cornell et al. [33].

45% methanol/1% acetic acid/54% water at 0.4 ml/min. Derivatized pyruvate was detected by fluorescence detection with excitation at 336 nm and emission at 420 nm (Rooseboom et al., 2000). Incubations were also performed in the absence of *Se*-(4-methylbenzyl)-L-selenocysteine to check the pyruvate formation from cysteine *S*-conjugates by GTK/β-lyase. None of the investigated ligands gave rise to pyruvate formation at the concentrations used. Non-enzymatic pyruvate formation from either *Se*-(4-methylbenzyl)-L-selenocysteine or the cysteine *S*-conjugates was not observed either under these conditions, with the exception of glutamine. IC_{50}-values were determined from the concentration-dependent inhibition by probit-analysis.

Table 3
Inhibition of amino acids and cysteine *S*-conjugates of the β-elimination reaction of *Se*-(4-methylbenzyl)-L-cysteine by rat GTK/β-lyase

Compound	IC_{50} (mM)[a]	Inhibition at 3 mM (%)
L-Glutamine	n.d.	n.d.
L-Phenylalanine	0.48 ± 0.05	91 ± 7
D-Phenylalanine	–	n.s.
S-Methyl-L-cysteine	–	40 ± 5
S-Carbamyl-L-cysteine	0.88 ± 0.10	80 ± 10
S-Phenyl-L-cysteine	0.91 ± 0.12	85 ± 5
S-(2-Nitrophenyl)-L-cysteine	–	20 ± 4
S-(2,4-Dinitrophenyl)-L-cysteine	0.18 ± 0.08	95 ± 5
S-(2-Nitro-4-carboxyphenyl)-L-cysteine	–	n.s.
S-(4-Methoxyphenyl)-L-cysteine	–	15 ± 5
S-Benzyl-L-cysteine	–	10 ± 7
S-(4-Methylbenzyl)-L-cysteine	–	12 ± 5
S-(4-Methoxybenzyl)-L-cysteine	–	n.s.

The inhibition by glutamine could not be determined (n.d.) due to spontaneous formation of pyruvate.

[a] IC_{50}-values were determined by probit-analysis of inhibitions observed at 0.1, 0.3, 1 and 3 mM of compound; n.s., not significant; n.d., not determined due to spontaneous formation of pyruvate.

3. Results and discussion

3.1. Inhibition studies

As indicated in Table 3, four of the studied amino acids and cysteine conjugates were able to produce more than 50% inhibition of the β-elimination reaction of *Se*-(4-methylbenzyl)-L-selenocysteine in the concentration range studied, enabling assessment of an IC_{50}-value. *S*-(2,4-Dinitrophenyl)-L-cysteine produced the strongest inhibition, with an IC_{50}-value of 0.18 ± 0.10 mM. L-Phenylalanine was slightly less inhibitory, having an IC_{50}-value of 0.48 ± 0.05 mM. The absence of any inhibitory effect of D-phenylalanine is indicative for the absolute stereoselectivity of GTK/β-lyase. *S*-Carbamyl-L-cysteine and *S*-phenyl-L-cysteine showed comparable inhibition having IC_{50}-values of 0.88 and 0.91 mM, respectively. The other compounds produced less than 50% inhibition at the highest concentration studied. The inhibition by L-glutamine could not be determined due to spontaneous formation of pyruvate, the measured product resulting from β-elimination of *Se*-(4-methylbenzyl)-L-selenocysteine by GTK/β-lyase.

3.2. Alignment

Sequence similarity searches of crystallized protein structures showed that the sequence of rat renal GTK/β-lyase (accession number Q08415) displayed the highest homology with *T. thermophilus* aspartate aminotransferase (tAAT; PDB-identifier 1BKG (2.6 Å resolution) [21]) and *T. cruzi* tyrosine aminotransferase (tTAT; PDB-identifier 1BW0 (2.5 Å resolution) [22]). Like rat GTK/β-lyase, both enzymes have been classified as γ-group members of the AT I subfamily of PLP-dependent enzymes on basis of sequence similarity and 3D-structure [4,5], and they displayed 30 and 17% sequence identity with rat GTK/β-lyase, respectively. The sequence identity between tAAT and tTAT was 25%, indicating that high structural conservation can exist despite low sequence identity. The alignment of rat GTK/β-lyase with tAAT and tTAT, in which both secondary structure elements and conserved residues are indicated, is depicted in Fig. 3. The functional role of the various conserved residues will be discussed below. As listed in Table 4, most secondary structure elements of the GTK/β-lyase homology model, especially those defining the PLP- and ligand-binding site, were found to be of "high" and "excellent" quality. Residues 1–31 of rat GTK/β-lyase have been omitted from the alignment and modeling procedure, because of the absence of any structural information from the templates. This, however, does not affect the quality of the rat GTK/β-lyase model regarding ligand-binding, as these residues are not part of the active site. Another homologue of rat GTK/β-lyase, an aminotransferase from *Pyrococcus horiskoshii*, was very recently crystallized (PhAT) [34]. This structure was not included in the study as the overall 3D-structure of PhAT is almost identical to that of tAAT: some short insertions and deletions were found only in loop-regions located on the surface of the protein. Furthermore, the sequence identity of PhAT with rat GTK/β-lyase was lower (28%) than that observed for tAAT (30%). The sequence identity between tAAT and PhAT was 41%.

Table 4
Quality of the modeled secondary structure elements of rat GTK/β-lyase based on its sequence homology with tAAT and tTAT (Fig. 2), and on the structural conservation between the templates

Element	Domain	Residue no.	Quality
H0	N-terminal segment	42–45	Low
H1	Small domain	49–55	Fair
a′	Small domain	64–67	High
H2	Large domain	78–89	Fair
H3	Large domain	104–118	Excellent
a	Large domain	128–131	Fair
H5	Large domain	133–145	Excellent
b	Large domain	151–156	High
H6	Large domain	161–168	High
c	Large domain	172–177	High
H7	Large domain	198–202	Fair
d	Large domain	209–215	Excellent
H8	Large domain	227–240	Excellent
e	Large domain	243–247	Excellent
f	Large domain	273–278	High
g	Large domain	291–294	High
H11	Large domain	297–308	High
H12	Large domain	316–327	Excellent
H13	Small domain	334–361	Fair
b′	Small domain	373–377	High
H15	Small domain	397–406	Fair
c′	Small domain	410–414	High
d′	Small domain	430–433	Excellent
H16	Small domain	439–457	Excellent

Qualities were assigned as outlined in Section 2.

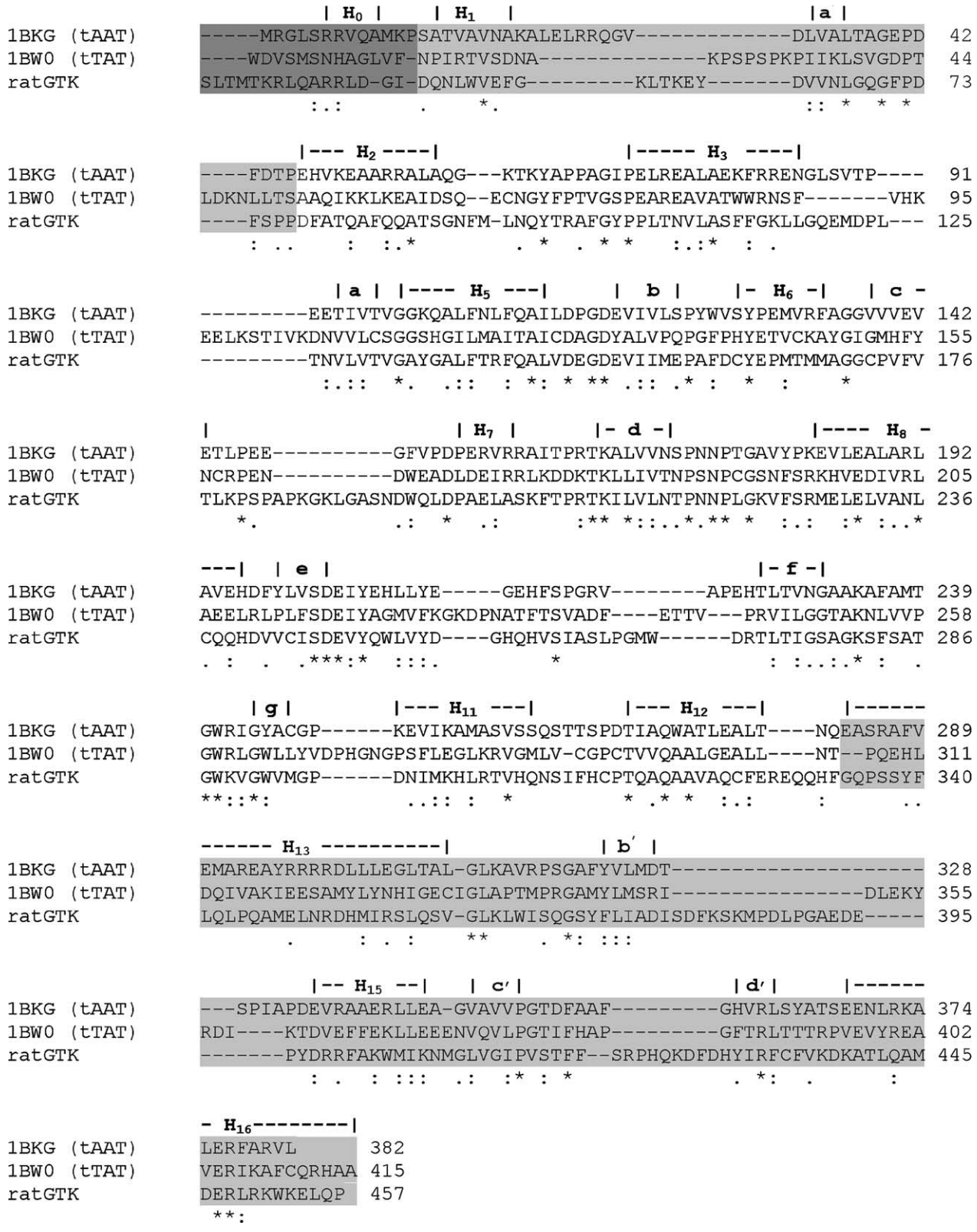

Fig. 3. Alignment of rat GTK/β-lyase with *Thermus thermophilus* aspartate aminotransferase (tAAT; PDB-identifier 1BKG) and *Trypanosoma cruzi* tyrosine aminotransferase (tTAT; PDB-identifier 1BW0). Residues shaded dark and light gray are part of the N-terminal segment and small domain, respectively. Non-shaded amino acids form the large domain of the enzymes. α-Helical structures, denoted H_0–H_{16}, are numbered in accordance with secondary structure elements present in aspartate aminotransferases and is analogous to that used for 1BKG and 1BW0. β-Strands present in the small domain and large domain are, respectively, named a′–d′ and a–g. Residue numbering corresponds with that of the crystal structures. An asterisk (∗) denotes a fully conserved residue (see also Table 1).

3.3. The GTK/β-lyase homology model

Comparative modeling of the rat GTK/β-lyase apoprotein with Modeller 4.0 resulted in 10 models, which only differed significantly in the structure of the non-aligned loop-regions. The model displaying the best stereochemical quality as determined by PROCHECK [30], and possessing extended loop conformations, was chosen for further modeling. In this model the backbone Φ and Ψ dihedral angles of 98% of residues were located within the generously allowed regions (80% core) of the Ramachandran plot. The model furthermore contained three *cis*-prolines in each monomer. Of these residues Pro^{157} and Pro^{220} are conserved as *cis*-prolines in the whole AT I subfamily, whereas the conservation of Pro^{217} as a *cis*-proline is specific for the γ-group of this subfamily [22]. Fig. 4 displays the overall fold and subunit-domains of the rat GTK/β-lyase homology model. The secondary structure elements, of which each domain is composed, are also depicted in Fig. 3.

3.4. Overall quality rat GTK/β-lyase homology model after MD

Final rms-values obtained for the Cα-trace of the studied ligand–enzyme complexes after 100 ps of MD at 300 K were small, varying between 1.3 and 1.4 Å. The complexes were stable for at least the last 20 ps of the MD simulation. PROCHECK analysis of the different complexes, after minimization of the final structure resulting from MD, demonstrated that the GTK/β-lyase model still possessed good stereochemical quality [30]. At least 97% of backbone Φ and Ψ dihedral angles of the residues were located within the generously allowed regions of the Ramachandran plot (70% core).

3.5. The PLP-binding site

Fig. 5 displays an orientation of PLP in the cofactor-binding site representative for those obtained after MD and minimization of the studied ligand–enzyme complexes. Comparison of the PLP-binding site of rat GTK/β-lyase with that of the templates tAAT and tTAT revealed the presence of conserved residues that anchor the cofactor to the large domain of the enzyme. In Table 1, these residues are listed along with their function. Only two residues are invariant within the α-family of PLP-enzymes: Lys^{281} and Asp^{247} [10]. Lys^{281} forms the internal aldimine with PLP, whereas Asp^{247} stabilizes the positive charge on the pyridinium atom of the cofactor. The latter interaction facilitates proton abstraction at Cα of substrates by enhancing the electron-withdrawing capacity of PLP [35]. The side chain conformation of Asp^{247} in the rat GTK/β-lyase model was found to be held in place via a hydrogen bond with the hydroxyl-group of Tyr^{162}, an interaction conserved in the

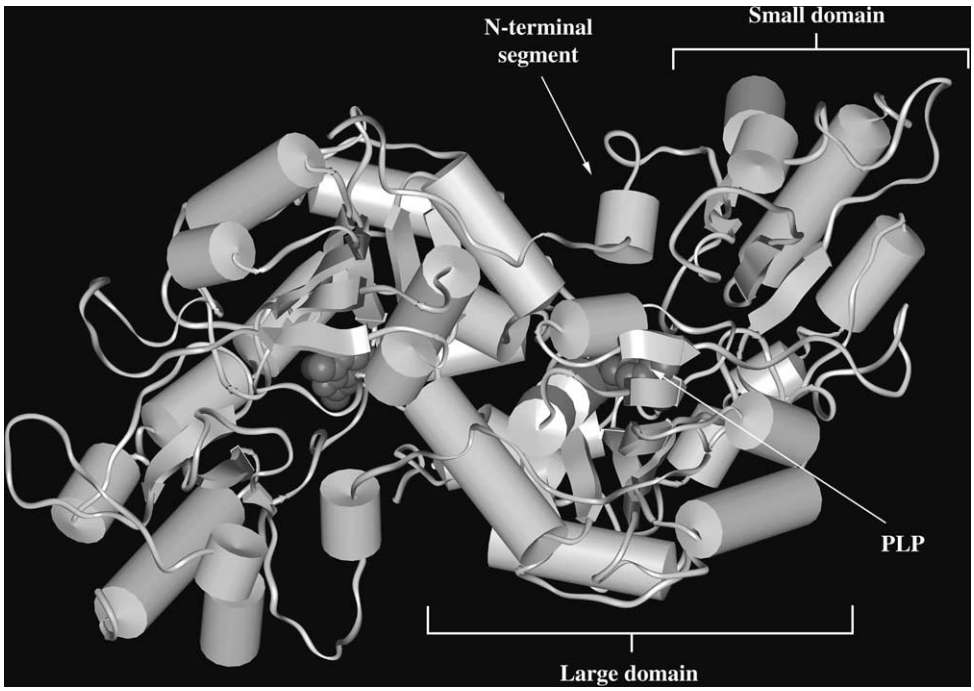

Fig. 4. Topology of the homodimeric rat GTK/β-lyase protein model. The three different domains, of which each subunit is composed, are indicated in the monomer located on the right. The cofactor is shown in CPK representation and is located at the subunit- and domain-interface, as is the ligand-binding site. Strands of β-sheets are shown as arrows, and α-helices are represented by cylinders. The N-terminal segment consists of a single helix and coil, whereas the small domain contains four α-helices and four β-strands. The invariant seven-stranded β-sheet of the large domain is sandwiched between eight α-helices.

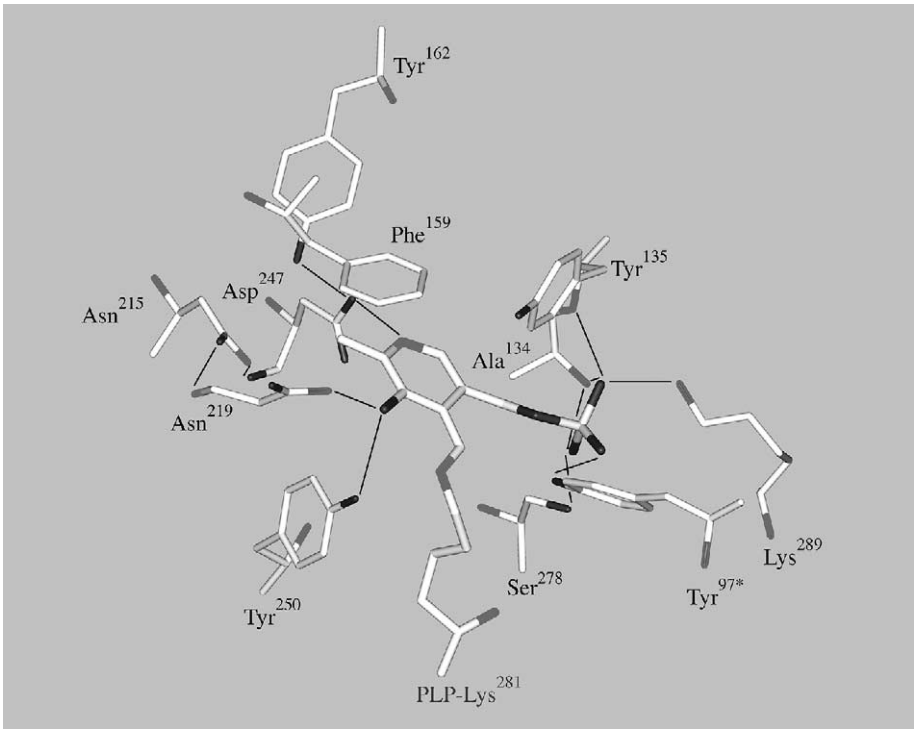

Fig. 5. Representative orientation of PLP and its interaction residues in the PLP-binding site of rat GTK/β-lyase. Lys^{281} was covalently bound to PLP by means of a Schiff base. Residues directly interacting with the cofactor via hydrogen bonds or salt bridges (both indicated by thin lines) included: Ala^{134}, Tyr^{135}, Asn^{219}, Asp^{247}, Tyr^{250}, Ser^{278}, Lys^{289} and Tyr^{97*} (∗ denotes a residue from the other subunit). Phe^{159} displayed π–π-stacking interaction with the aromatic moiety of PLP, whereas both Asn^{215} and Tyr^{162} were found to stabilize the conformation of Asp^{247}.

templates. The carbamoyl nitrogen of Asn^{215} appeared to additionally stabilize the position of Asp^{247} via a hydrogen bond with the carbonyl oxygen of Asp^{247}. PLP-binding residues conserved within the AT I subfamily are Asn^{219}, Tyr^{250}, and Tyr^{97*} (∗ denotes a residue originating from the other subunit). Tyr^{97*} forms a hydrogen bond with the PLP 5′-phosphate-group, whereas Asn^{219} and Tyr^{250} form hydrogen bonds with the phenolic oxygen (O3; Table 2) of the cofactor. Another residue involved in PLP-binding was found to be Phe^{159}, providing π-stacking interaction with the ring of PLP. In the templates this residue is present as Phe^{138} (1BW0) and Trp^{125} (1BKG). Apart from being stabilized by Ser^{278}, Lys^{289}, and Tyr^{97*}, the phosphate-group of PLP was found to additionally interact with the backbone nitrogen atoms of Ala^{134} and Tyr^{135}.

3.6. The ligand-binding site

MD studies on the ligand–enzyme complexes investigated (Fig. 2) revealed a common binding mode for the amino acid moiety of the ligands (Figs. 6 and 7). Key residues anchoring the amino acid moiety in the observed orientation were found to include Arg^{432} and Asn^{219}, which both hydrogen bonded with the ligand α-carboxylate-group. Arg^{432} is conserved throughout the whole α-family (Table 1) and its role in substrate binding has been extensively studied both in AATs and tTAT by means of crystallization and mutation studies [21,22,36,37]. As found in other aminotransferases [38], the stability of the interaction between the ligand α-carboxylate-group and Arg^{432} and Asn^{219} was enhanced by a hydrogen bond between the latter two residues. In the ligand-free enzyme, the hydrogen bond linkage between Arg^{432}, Asn^{219}, and O3 of PLP (Table 2), results in a strained torsion of the imine–pyridine bond, which lowers the pK_a value of the imine nitrogen. Upon binding of a ligand α-carboxylate-group to Arg^{432} and Asn^{219}, the strain is relaxed and the pK_a increased, enabling proton transfer from the protonated ligand amino-group to the imine nitrogen of PLP [39]. Apart from Asn^{219}, the conformation of Arg^{432} was found to be further fixed in position by Phe^{373}, displaying parallel stacking with the guanidinium group of Arg^{432} [40]. In *Escherichia coli* AAT, Phe^{360} fulfills this role [37], whereas Tyr^{322} and Tyr^{345} constitute the equivalent residues in, respectively, tAAT and tTAT. Unique to rat GTK/β-lyase, when comparing its 3D-structure to that of the templates, was the involvement of Asn^{50} located in the H_1-helix in the binding of the α-carboxylate-group through a hydrogen bond. Gly^{70} was additionally found to form a hydrogen bond with the ligand α-carboxylate-group via its backbone nitrogen. The presence of this interaction has also been suggested by modeling studies on the corresponding glycine residue in tTAT [37], and was furthermore observed in the crystal structures of pig and *E. coli* AATs [11,28]. In the case of the latter aminotransferases, the conserved

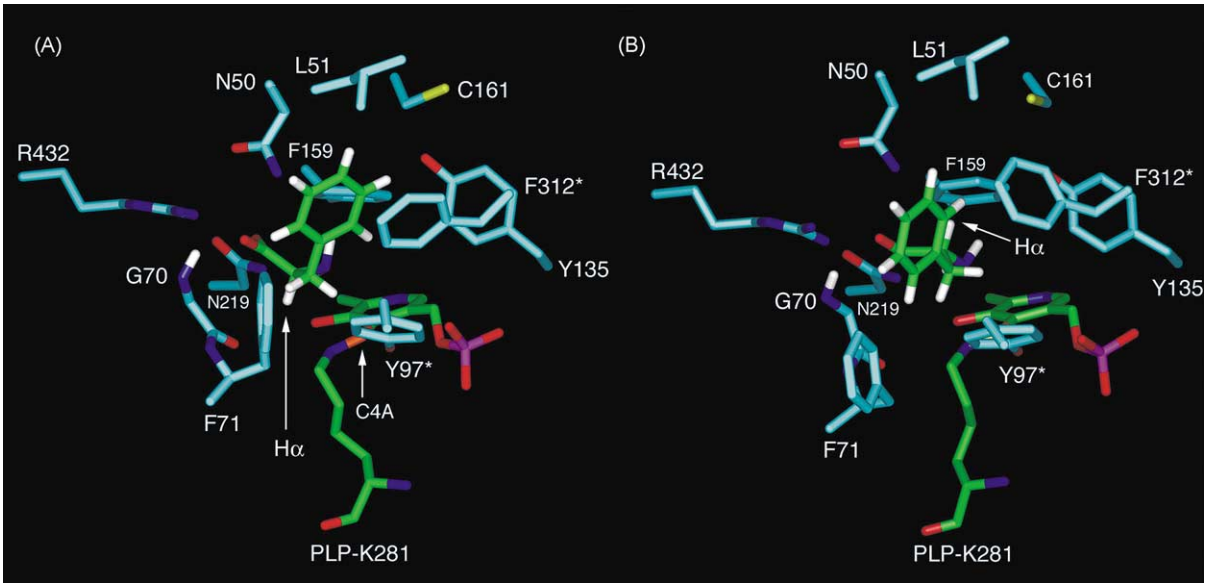

Fig. 6. Preferred binding mode of L-phenylalanine (A) and D-phenylalanine (B) in the active site of rat GTK/β-lyase, as deduced from MD studies. Carbon atoms of active site residues are colored blue, whereas those of the cofactor PLP and docked ligand are colored green. Residues originating from the other subunit are denoted with an asterisk (∗). The reactive center of PLP, C4A, is also indicated together with the α-proton of the ligands. It can be observed that the proton on Cα is directed away from the PLP–Lys^{281} Schiff base in the case of D-phenylalanine. This orientation of Hα in D-phenylalanine hinders α-proton abstraction by Lys^{281}, which is an essential step in the conversion of the external aldimine to the quinonoid [7] (Fig. 2), and may therefore explain why D-configured amino acids are not metabolized by GTK/β-lyase.

G-X-G sequence (present as Gly^{68}–Gln^{69}–Gly^{70} in rat GTK) has been found to play an important role in the transition of the protein from the open to closed conformation upon ligand-binding [11]. The apparent tight binding of the ligand α-carboxylate-group by Arg^{432}, Asn^{219}, Asn^{50} and Gly^{70}, resulted in comparable binding orientations of the α-NH_2 group of the ligands. The nitrogen atom of the latter was found to be positioned almost directly above the reactive center C4A of PLP, with a small deviation in the direction of O3 of PLP (Figs. 6 and 7). The distances observed between the α-nitrogen atom and C4A are listed in Table 5 for the different ligand–enzyme complexes.

Docking studies with GTK/β-lyase revealed two possible binding orientations for the ligand side chains. In the first orientation, only found for small ligands, the side chain extended into the pocket directly above the cofactor PLP. In the second orientation, the ligand side chain extended into the substrate access channel, which runs parallel to the α-helix H_1. In both orientations, the ligands were found to be shielded from the solvent by an extensive hydrogen bonding network involving residues at both sides of the substrate access channel: Glu^{54}, Gln^{69}, Asp^{42}, Asn^{96*}, Arg^{99*}, Lys^{437} (∗ denotes a residue originating from the other subunit). Table 5 lists the contact residues, whose side chains are involved in the binding of the ligands investigated. The specifics of the binding mode of these compounds and their correlation with experimental results from competition studies (Table 3) are described in the following paragraphs.

3.6.1. *Binding modes of* D- *and* L-*phenylalanine*

MD studies on L-phenylalanine in the active site of GTK/β-lyase showed that, in the preferred binding mode, the aromatic ring interacted with residues belonging to the pocket located directly above PLP (Fig. 6A). This pocket was found to be of a highly aromatic and hydrophobic character, corresponding with the high inhibitory potency of L-phenylalanine observed in the competition experiments with GTK/β-lyase (Table 3). Tight binding of the L-phenylalanine side chain was found to be mainly provided by π–π-stacking interactions with Phe^{312*} and by the presence of a hydrogen bond between the Nε-H of Asn^{50} and one of the π-faces of the ligand phenyl-ring. The latter interaction, i.e. hydrogen bonding interactions with π-acceptors, are commonly observed in proteins [41]. Van der Waals interactions of the ligand phenyl-ring were predominantly observed with Phe^{159}, Tyr^{135}, Phe^{71}, Tyr^{97*} and Leu^{51} (Table 5). The α-carboxy-group of L-phenylalanine displayed forked hydrogen bonds with Arg^{432}. Hydrogen bonds were also present between this moiety and Gly^{70}, Asn^{50}, and Asn^{219}.

GTK/β-lyase is known to be selective for L-configured amino acids. This finding was supported by the competition studies in which D-phenylalanine showed no significant inhibition of GTK/β-lyase at concentrations up to 3 mM. MD studies indicated that D-phenylalanine could only be docked in the GTK/β-lyase active site in a binding mode that differed strongly from that observed for the L-isomer (Fig. 6B). To enable hydrogen bond formation between its

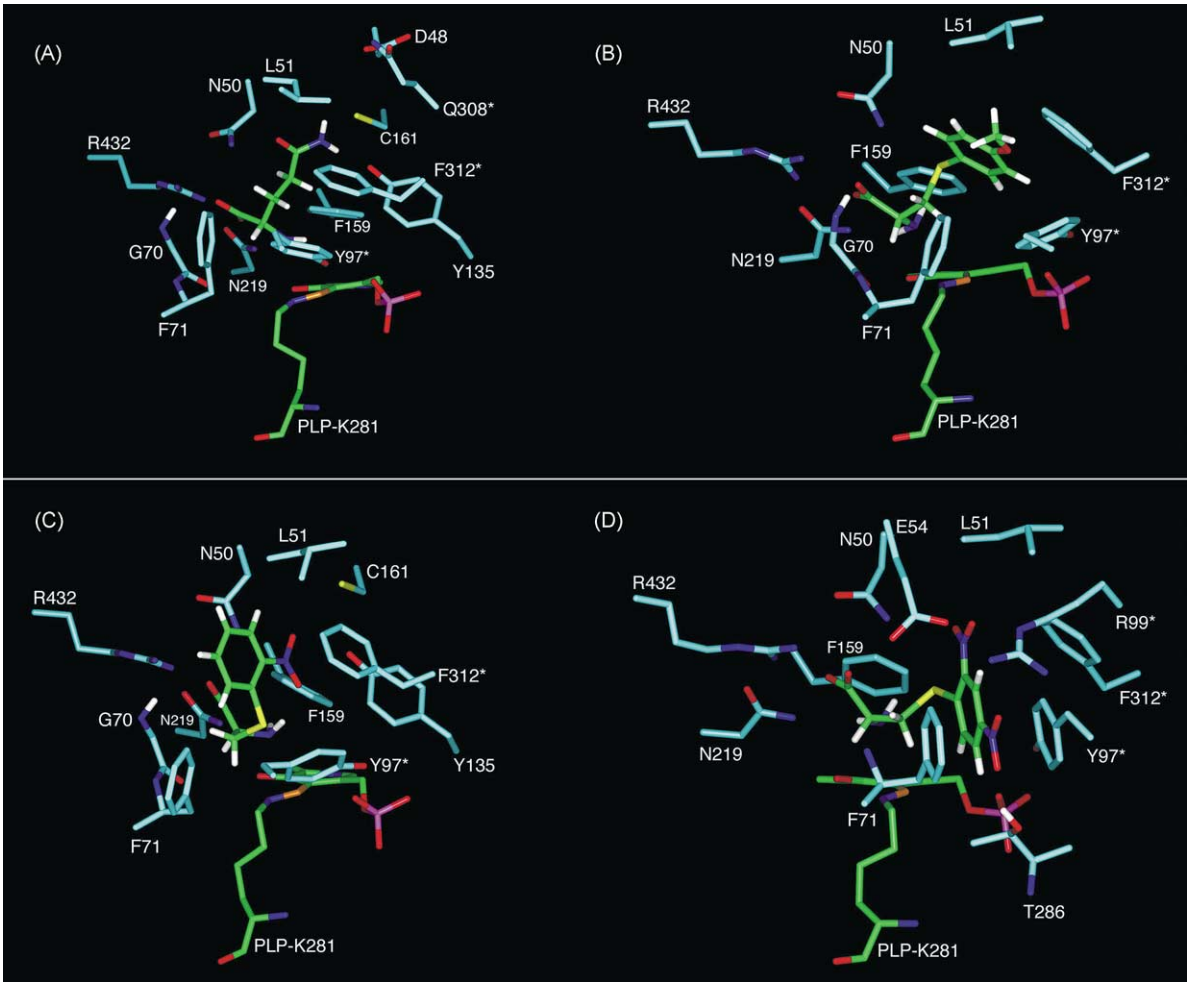

Fig. 7. Preferred binding mode of several ligands in the GTK/β-lyase active site, as deduced from MD studies. Carbon atoms of active site residues are colored blue, whereas those of the cofactor PLP and docked ligand are colored green. The reactive center of PLP, C4A, is shown in orange. Residues originating from the other subunit are denoted with an asterisk (∗). Illustrated ligands are: (A) glutamine; (B) *S*-(4-methoxyphenyl)-L-cysteine; (C) *S*-(2-nitrophenyl)-L-cysteine; (D) *S*-(2,4-dinitrophenyl)-L-cysteine.

α-carboxylate-group and Arg^{432}, Asn^{50}, and Asn^{219}, the side chain of D-phenylalanine could not overlap with that of L-phenylalanine but was directed towards the substrate access channel. As a result, D-phenylalanine was unable to form either π-stacking interactions with Phe^{312*} or a hydrogen bond with Asn^{50}, in contrast to L-phenylalanine (Table 5). Due to steric restrictions, D-phenylalanine could neither form a hydrogen bond with Gly^{70}. Compared to the L-isomer, D-phenylalanine displayed less Van der Waals contacts with the hydrophobic interaction residues Phe^{159} and Tyr^{135}. Instead, the aromatic ring of D-phenylalanine was located in close vicinity of the charged atoms of residues Glu^{54} and Arg^{99*}. The localization of the D-phenylalanine side chain in the more hydrophilic pocket formed by the substrate access-channel, combined with the loss of π-stacking interaction and several hydrogen bonds, may explain the lack of inhibition of GTK/β-lyase by D-phenylalanine at a concentration of 3 mM (Table 3).

3.6.2. Binding modes of L-glutamine, S-carbamyl- and S-methyl-L-cysteine

L-Glutamine, *S*-carbamyl-L-cysteine and *S*-methyl-L-cysteine were found to adopt similar binding orientations in the active site of rat GTK/β-lyase (Fig. 7A), which were largely comparable to that of L-phenylalanine. As listed in Table 5, active site residues forming hydrogen bonds with the ligand carbamoyl-group, or *S*-atom in the case of *S*-methyl-L-cysteine, included Asn^{50}, Tyr^{135}, Cys^{162}, and Gln^{308*}. Tyr^{135} and Gln^{308*} correspond with Lys^{101} in tAAT and Arg^{292*} in *E. coli* AATs, respectively. Both bind the ω-carboxylate-group of its endogenous substrate aspartate [21,29].

As shown in Table 3, *S*-carbamyl-L-cysteine was better able to inhibited rat GTK/β-lyase than *S*-methyl-L-cysteine. The less potent inhibition observed for *S*-methyl-L-cysteine may be attributed to the fact that, compared to *S*-carbamyl-L-cysteine, this compound lacks two hydrogen bonds

Table 5
Active site residues in the rat GTK homology model, whose side chains interact with the investigated ligands

	L-Phenylalanine	D-Phenylalanine	Glutamine	*S*-Carbamyl-L-cysteine	*S*-Methyl-L-cysteine	*S*-Phenyl-L-cysteine	*S*-(4-Methoxy-phenyl)-L-cysteine	*S*-(2-Nitrophenyl)-L-cysteine	*S*-(2,4-Dinitrophenyl)-L-cysteine	*S*-(4-Carboxy-2-nitro-phenyl-L-cysteine	*S*-Benzyl-L-cysteine	*S*-(4-Methylbenzyl)-L-cysteine	*S*-(4-Methoxy-benzyl)-L-cysteine
Asp^{48}			W	W									
Asn^{50}	Hα/Hs[a]	Hα	Hα/Hs	Hα/Hs	Hα/Hs (W)[b]	Hα/Hs	Hα/Hs	Hα	Hα/Hs	Hα/Hs	Hα	Hα/Hs	Hα
Leu^{51}	W	W	W	W	W	W	W	W	W	W	W	W	W
Glu^{54}		W				W	W	W	W	W	W	W	W
Phe^{55}											W	W	W
Gln^{69}												W	
Gly^{70}	Hα	W	Hα	Hα	Hα	Hα	Hα	Hα	Hα	Hα	Hα	Hα	Hα
Phe^{71}	W	W	W	W	W	T–π	T–π	W	W	W	W	W	W
Tyr^{135}	W	W	Hs	Hs	W (Hs)[b]	W	W	Hs	W	W	Hs	W	Hs
Phe^{159}	W	W	W	W	W	W	W	W	W	W	W	W	W
Cys^{161}			Hs (W)[b]	Hs (W)[b]				W					
Asn^{219}	Hα	Hα	Hα	Hα	Hα	Hα	Hα	Hα	Hα	Hα	Hα	Hα	Hα
Tyr^{250}	W	W	W	W	W	W	W	W	W	W	W	W	W
Thr^{286}									Hs	Hs			
Phe^{373}	W	W	W	W	W	W	W	W	W	W	W	W	W
Arg^{432}	Hα	Hα	Hα	Hα	Hα	Hα	Hα	Hα	Hα	Hα	Hα	Hα	Hα
Gln^{96}*									W	W	W	W	W
Tyr^{97}*	W	W	W	W	W	W	W	W	π–π/Hs	π–π/Hs	W	W	W
Arg^{99}*		W				W	W	W	E	Hs	W	W	W
Gln^{308}*			W (Hs)[b]	W (Hs)[b]									
Phe^{312}*	π–π	W	W	W	W	W	W	W	W	W	W	W	W
C4A-N (Å)	3.00	3.05	3.13	3.05	2.98	3.10	3.26	3.09	3.00	3.68	2.99	3.05	3.01

The observed type of interaction is indicated by: W, Van der Waals interaction; Hα, hydrogen bond with ligand α-amino acid group; Hs, hydrogen bond with ligand side chain; π–π, planar π-stacking interaction; T–π, perpendicular or T-shaped π-stacking interaction; E, electrostatic charge interaction with ligand lone pair. The distance between the reactive site of PLP and the α-nitrogen atom of the ligands (C4A-N) is listed as well.

[a] H-bond with the π-face of the ligand aromatic moiety.

[b] Alternative binding mode.

(Table 5). Additionally, the smaller *S*-methyl-L-cysteine was engaged in fewer Van der Waals contacts (Table 5). *S*-Carbamyl-L-cysteine was found capable of forming three hydrogen bonds through its carbamoyl-group. L-Phenylalanine, in comparison, displayed more hydrophobic interactions as well as π-stacking with Phe^{312*} and a hydrogen bond with Asn^{50} (Table 5). Although the exact energy contributions of these specific types of interactions are difficult to determine, studies have indicated that the energy gain of planar π-stacking is approximately 3 kcal/mole [42]. This is in the same order of magnitude as the energy contribution of a hydrogen bond between polar groups, or the N-H/π-interaction as observed between Asn^{50} and L-phenylalanine [41,43]. As such it was expected that *S*-carbamyl-L-cysteine had at least an inhibitory potency comparable to that of L-phenylalanine. Competition studies, however, indicated that hydrophobic effects are of dominating importance as L-phenylalanine is a more potent inhibitor than *S*-carbamyl-L-cysteine (Table 3). This is probably attributable to additional factors, such as the desolvation energy of the ligands, which could not be included in the MD studies.

3.6.3. Binding modes of S-phenyl substituted L-cysteine conjugates

During the MD simulation, *S*-phenyl-L-cysteine adopted a conformation such that the phenyl-ring was located in a position similar to that of D-phenylalanine. But due to its higher flexibility the aromatic moiety was able to rotate 90°, enabling T-shaped π-stacking with Phe^{71}. T-shaped π-stacking is reported to be somewhat less favorable than planar π-stacking as observed for L-phenylalanine, but still results in an energy gain of approximately 2 kcal/mole [42]. Additionally, a hydrogen bond between Asn^{50} and its sulfur-atom was observed.

S-(4-Methoxyphenyl)-L-cysteine (Fig. 7B) showed virtually identical interactions with GTK/β-lyase compared to *S*-phenyl-L-cysteine (Table 5), as these compounds differed only slightly in binding orientation. The 4-substituent of *S*-(4-methoxyphenyl)-L-cysteine extended further into the substrate access channel. The lipophilic methyl-group was consequently located in close vicinity of the charged atoms of Glu^{54} and Arg^{99*}. The unfavorable position of the 4-substituent may explain the lower inhibition observed for *S*-(4-methoxyphenyl)-L-cysteine compared to *S*-phenyl-L-cysteine (Table 3).

The preferred binding mode of *S*-(2-nitrophenyl)-L-cysteine differed substantially from that observed for *S*-phenyl-L-cysteine (Fig. 7C). *S*-(2-Nitrophenyl)-L-cysteine adopted a folded conformation and, as such, did not display π-stacking interactions with aromatic residues of GTK/β-lyase. Neither was the sulfur-atom able to form a hydrogen bond. The 2-nitrogroup of the ligand was located directly above the cofactor, hydrogen bonding with the hydroxyl-group of Tyr^{135}. This placed the highly polar substituent in the near vicinity the hydrophobic residues Phe^{312*} and Phe^{159}. At an inhibitor concentration of 3 mM, GTK/β-lyase inhibition was decreased from 85 to 20% upon introduction of a 2-nitro-group to *S*-phenyl-L-cysteine (Table 3). The observed loss of π-stacking interactions, and the unfavorable position of the 2-nitro-group may explain this reduction in inhibitory potency.

MD simulations revealed that the introduction of an additional nitro-group to *S*-(2-nitrophenyl)-L-cysteine at the *p*-position again had a dramatic effect on the observed binding orientation of the compound (Fig. 7D). The aromatic ring of *S*-(2,4-dinitrophenyl)-L-cysteine exhibited planar π-stacking interactions with Tyr^{97*}, and its 4-nitro-group was directed towards the access channel. The latter was engaged in hydrogen bonds with both the backbone NH of Tyr^{97*} and the hydroxyl-group of Thr^{286}. Asn^{50} additionally formed a hydrogen bond with the sulfur-atom of *S*-(2,4-dinitrophenyl)-L-cysteine. The difference in binding mode, and the advantageous interactions of especially the 4-nitro-group corresponds well with the higher inhibitory potency of *S*-(2,4-dinitrophenyl)-L-cysteine compared to the 2-nitro compound (Table 3). The larger number of favorable interactions (Table 5) also explains the preference of GTK/β-lyase for binding *S*-(2,4-dinitrophenyl)-L-cysteine over the unsubstituted *S*-phenyl-L-cysteine (Table 3).

Another *S*-phenyl-L-cysteine conjugate investigated was *S*-(4-carboxy-2-nitrophenyl)-L-cysteine. This compound could also be docked in the active site of GTK/β-lyase, but only in an orientation resembling that of *S*-(2,4-dinitrophenyl)-L-cysteine. In the case of *S*-(4-carboxy-2-nitrophenyl)-L-cysteine, however, this binding mode resulted in an unfavorable interaction between the negative charges of the 4-carboxy group of the ligand and Glu^{54}. Electrostatic repulsion was similarly observed with the carbamoyl-oxygen of Asn^{96*} as reflected by the loss of its hydrogen bond with Arg^{99*} which participates in shielding the active site from the solvent layer. The observed unfavorable interactions may explain the fact that *S*-(4-carboxy-2-nitrophenyl)-L-cysteine did not significantly inhibit GTK/β-lyase (Table 3).

3.6.4. Binding modes of S-benzyl substituted L-cysteine conjugates

The *S*-benzyl substituted L-cysteine conjugates were found to adopt similar binding modes. Compared to *S*-phenyl-L-cysteine, the aromatic ring of the benzylic ligands extended further into the substrate access channel. As a consequence, the benzyl moiety displayed less hydrophobic interactions and had no T-shaped π-stacking with Phe^{71} (Table 5). This corresponds with the lower inhibition of GTK/β-lyase by (4-substituted) *S*-benzyl-L-cysteine compared to *S*-phenyl-L-cysteine (Table 3). The sulfur-atom of the benzylic ligands was found able to interact with either Tyr^{135} or Asn^{50}. As for *S*-(4-methoxyphenyl)-L-cysteine, the 4-substituent of *S*-(4-methylbenzyl)- and *S*-(4-methoxybenzyl)-L-cysteine had close Van der Waals contacts with

the charged atoms of the salt-bridge partners Glu^{54} and Arg^{99*}.

4. Conclusions

In this study we have described the development of the first homology model for cytosolic rat kidney GTK/β-lyase. The current model possesses good stereochemical quality and appears to be consistent with obtained experimental data on the inhibitory potency of ligands. The cofactor-binding site of rat GTK/β-lyase was found to be highly conserved, as were two of the most important residues involved in anchoring the ligand α-amino acid group in a position enabling metabolism of L-amino acids: Arg^{432} and Asn^{219}. Other residues specific for rat GTK/β-lyase that may interact with the α-carboxylate-group of ligands were Asn^{50} and Gly^{70}. Two distinct pockets are proposed to be involved in binding of the ligand side chain. The first binding site involves a small pocket located directly above the cofactor PLP, and was of a highly hydrophobic and aromatic character. The second and larger binding site, which was part of the substrate access channel, was of a more hydrophilic character and notably involved the salt bridge partners Glu^{54} and Arg^{99*}. These residues originate from different subunits. Prominent residues involved in binding ligand side chains included Leu^{51}, Phe^{71}, Tyr^{135}, Phe^{373} and Phe^{312*}. Due to the presence of the large number of aromatic residues, π-stacking interactions were often found to contribute to ligand-binding. In addition, Tyr^{135} and Asn^{50} seemed to play a role in hydrogen bonding to the sulfur-atom of cysteine-*S*-conjugates. This first homology model of rat GTK/β-lyase provides a starting point for further elucidation of the role of active site residues involved in ligand-binding by means of site-directed mutagenesis studies. Insight in the binding of ligands to GTK/β-lyase may ultimately lead to the rational design of more selective substrates or inhibitors.

References

[1] A.J. Cooper, A. Meister, Isolation and properties of a new glutamine transaminase from rat kidney, J. Biol. Chem. 249 (1974) 2554–2561.

[2] A.J.L. Cooper, A. Meister, Comparative studies on glutamine transaminases from rat tissues, Comp. Biochem. Physiol. 69B (1981) 137–145.

[3] A.J.L. Cooper, Mechanisms of cysteine conjugate β-lyases, Adv. Enzymol. Relat. Areas Mol. Biol. 72 (1998) 199–238.

[4] P.K. Mehta, P. Christen, The molecular evolution of pyridoxal-5′-phosphate-dependent enzymes, Adv. Enzymol. Relat. Areas Mol. Biol. 74 (2000) 129–184.

[5] R.A. Jensen, W. Gu, Evolutionary recruitment of biochemically specialized subdivisions of Family I within the protein superfamily of aminotransferases, J. Bacteriol. 178 (1996) 2161–2171.

[6] H. Hayashi, Pyridoxal enzymes: mechanistic diversity and uniformity, J. Biochem. (Tokyo) 118 (1995) 463–473.

[7] J.N. Jansonius, Structure, evolution and action of vitamin B6-dependent enzymes, Curr. Opin. Struct. Biol. 8 (1998) 759–769.

[8] J.N. Commandeur, G.J. Stijntjes, N.P. Vermeulen, Enzymes and transport systems involved in the formation and disposition of glutathione *S*-conjugates. Role in bioactivation and detoxication mechanisms of xenobiotics, Pharmacol. Rev. 47 (1995) 271–330.

[9] J.L. Stevens, J.D. Robbins, R.A. Byrd, A purified cysteine conjugate β-lyase from rat kidney cytosol. Requirement for an α-keto acid or an amino acid oxidase for activity and identity with soluble glutamine transaminase K, J. Biol. Chem. 261 (1986) 15529–15537.

[10] R.A. John, Pyridoxal phosphate-dependent enzymes, Biochim. Biophys. Acta 1248 (1995) 81–96.

[11] A. Okamoto, T. Higuchi, K. Hirotsu, S. Kuramitsu, H. Kagamiyama, X-ray crystallographic study of pyridoxal 5′-phosphate-type aspartate aminotransferases from *Escherichia coli* in open and closed form, J. Biochem. (Tokyo) 116 (1994) 95–107.

[12] T. Clausen, R. Huber, B. Laber, H.D. Pohlenz, A. Messerschmidt, Crystal structure of the pyridoxal-5′-phosphate dependent cystathionine β-lyase from *Escherichia coli* at 1.83 A, J. Mol. Biol. 262 (1996) 202–224.

[13] M. Rooseboom, N.P. Vermeulen, J.N. Commandeur, Enzymatic pathways of β-elimination of chemopreventive selenocysteine *Se*-conjugates, Methods Enzymol. 348 (2002) 191–200.

[14] C. Jiang, W. Jiang, C. Ip, H. Ganther, J. Lu, Selenium-induced inhibition of angiogenesis in mammary cancer at chemopreventive levels of intake, Mol. Carcinogen. 26 (1999) 213–225.

[15] J. Lu, H. Pei, C. Ip, D.J. Lisk, H. Ganther, H.J. Thompson, Effect on an aqueous extract of selenium-enriched garlic on in vitro markers and in vivo efficacy in cancer prevention, Carcinogenesis 17 (1996) 1903–1907.

[16] E.M. Schaffer, J.Z. Liu, J. Green, C.A. Dangler, J.A. Milner, Garlic and associated allyl sulfur components inhibit *N*-methyl-*N*-nitrosourea induced rat mammary carcinogenesis, Cancer Lett. 102 (1996) 199–204.

[17] C. Ip, Z. Zhu, H.J. Thompson, D. Lisk, H.E. Ganther, Chemoprevention of mammary cancer with *Se*-allylselenocysteine and other selenoamino acids in the rat, Anticancer Res. 19 (1999) 2875–2880.

[18] J.N. Commandeur, I. Andreadou, M. Rooseboom, M. Out, L.J. de Leur, E. Groot, N.P. Vermeulen, Bioactivation of selenocysteine *Se*-conjugates by a highly purified rat renal cysteine conjugate β-lyase/glutamine transaminase K, J. Pharmacol. Exp. Ther. 294 (2000) 753–761.

[19] I. Andreadou, W.M. Menge, J.N. Commandeur, E.A. Worthington, N.P. Vermeulen, Synthesis of novel *Se*-substituted selenocysteine derivatives as potential kidney selective prodrugs of biologically active selenol compounds: evaluation of kinetics of β-elimination reactions in rat renal cytosol, J. Med. Chem. 39 (1996) 2040–2046.

[20] M.J. De Groot, N.P. Vermeulen, Modeling the active sites of cytochrome P450s and glutathione *S*-transferases, two of the most important biotransformation enzymes, Drug Metab. Rev. 29 (1997) 747–799.

[21] T. Nakai, K. Okada, S. Akutsu, I. Miyahara, S. Kawaguchi, R. Kato, S. Kuramitsu, K. Hirotsu, Structure of *Thermus thermophilus* HB8 aspartate aminotransferase and its complex with maleate, Biochemistry 38 (1999) 2413–2424.

[22] W. Blankenfeldt, C. Nowicki, M. Montemartini-Kalisz, H.M. Kalisz, H.J. Hecht, Crystal structure of *Trypanosoma cruzi* tyrosine aminotransferase: substrate specificity is influenced by cofactor binding mode, Protein Sci. 8 (1999) 2406–2417.

[23] A. Yamauchi, G.J. Stijntjes, J.N. Commandeur, N.P. Vermeulen, Purification of glutamine transaminase K/cysteine conjugate β-lyase from rat renal cytosol based on hydrophobic interaction HPLC and gel permeation FPLC, Protein Exp. Purif. 4 (1993) 552–562.

[24] I.S. Blaghbrough, B.W. Bycroft, D.C. Evans, P.N. Shaw, Inhibition of rat renal C-S lyase: assessment using kidney slice methodology, Drug Metabol. Drug Interact. 6 (1988) 303–316.

[25] B. Rost, C. Sander, Combining evolutionary information and neural networks to predict protein secondary structure, Proteins 19 (1994) 55–72.

[26] B. Rost, C. Sander, R. Schneider, PHD—an automatic mail server for protein secondary structure prediction, Comput. Appl. Biosci. 10 (1994) 53–60.
[27] A. Sali, T.L. Blundell, Comparative protein modelling by satisfaction of spatial restraints, J. Mol. Biol. 234 (1993) 779–815.
[28] S. Rhee, M.M. Silva, C.C. Hyde, P.H. Rogers, C.M. Metzler, D.E. Metzler, A. Arnone, Refinement and comparisons of the crystal structures of pig cytosolic aspartate aminotransferase and its complex with 2-methylaspartate, J. Biol. Chem. 272 (1997) 17293–17302.
[29] H. Ura, T. Nakai, S. Kawaguchi, I. Miyahara, K. Hirotsu, S. Kuramitsu, Substrate recognition mechanism of thermophilic dual-substrate enzyme, J. Biochem. (Tokyo) 130 (2001) 89–98.
[30] R. Laskowski, M. MacArthur, D. Moss, J. Thornton, PROCHECK: a program to check the stereochemical quality of protein structures, J. Appl. Cryst. 26 (1993) 283–291.
[31] P. Cieplak, W.D. Cornell, C. Bayly, P.A. Kollman, Application of the multimolecule and multiconformational RESP methodology to biopolymers: charge derivation for DNA, RNA, and proteins, J. Comp. Chem. 16 (1995) 1357–1377.
[32] C.I. Bayly, P. Cieplak, W.D. Cornell, P.A. Kollman, A well-behaved electrostatic potential based method using charge restraints for deriving atomic charges: the RESP model, J. Phys. Chem. 97 (1993) 10269–10280.
[33] W.D. Cornell, P. Cieplak, C.I. Bayly, P.A. Kollman, Application of RESP charges to calculate conformational energies, hydrogen bond energies, and free energies of solvation, J. Am. Chem. Soc. 115 (1993) 9620–9631.
[34] H. Ura, K. Harata, I. Matsui, S. Kuramitsu, Temperature dependence of the enzyme–substrate recognition mechanism, J. Biochem. (Tokyo) 129 (2001) 173–178.
[35] T. Yano, S. Kuramitsu, S. Tanase, Y. Morino, H. Kagamiyama, Role of Asp^{222} in the catalytic mechanism of *Escherichia coli* aspartate aminotransferase: the amino acid residue which enhances the function of the enzyme-bound coenzyme pyridoxal 5′-phosphate, Biochemistry 31 (1992) 5878–5887.
[36] C. Nowicki, G.R. Hunter, M. Montemartini-Kalisz, W. Blankenfeldt, H. Hecht, H.M. Kalisz, Recombinant tyrosine aminotransferase from *Trypanosoma cruzi*: structural characterization and site directed mutagenesis of a broad substrate specificity enzyme, Biochim. Biophys. Acta 1546 (2001) 268–281.
[37] A.T. Danishefsky, J.J. Onnufer, G.A. Petsko, D. Ringe, Activity and structure of the active-site mutants R386Y and R386F of *Escherichia coli* aspartate aminotransferase, Biochemistry 30 (1991) 1980–1985.
[38] T. Yano, T. Mizuno, H. Kagamiyama, A hydrogen-bonding network modulating enzyme function: asparagine-194 and tyrosine-225 of *Escherichia coli* aspartate aminotransferase, Biochemistry 32 (1993) 1810–1815.
[39] H. Mizuguchi, H. Hayashi, K. Okada, I. Miyahara, K. Hirotsu, H. Kagamiyama, Strain is more important than electrostatic interaction in controlling the pK_a of the catalytic group in aspartate aminotransferase, Biochemistry 40 (2001) 353–360.
[40] J.P. Gallivan, D.A. Dougherty, Cation–π interactions in structural biology, Proc. Natl. Acad Sci. U.S.A. 96 (1999) 9459–9464.
[41] T. Steiner, G. Koellner, Hydrogen bonds with π-acceptors in proteins: frequencies and role in stabilizing local 3D structures, J. Mol. Biol. 305 (2001) 535–557.
[42] G.B. McGaughey, M. Gagne, A.K. Rappe, π-Stacking interactions. Alive and well in proteins, J. Biol. Chem. 273 (1998) 15458–15463.
[43] M. Brandl, M.S. Weiss, A. Jabs, J. Suhnel, R. Hilgenfeld, C–H$\cdots$π-interactions in proteins, J. Mol. Biol. 307 (2001) 357–377.
[44] P.K. Mehta, T.I. Hale, P. Christen, Aminotransferases: demonstration of homology and division into evolutionary subgroups, Eur. J. Biochem. 214 (1993) 549–561.